Published in final edited form as:

Int J Cancer. 2016 August 1; 139(3): 712–718. doi:10.1002/ijc.30098.

Predictive imaging of chemotherapeutic response in a transgenic mouse model of pancreatic cancer

Ping Wang[1], **Byunghee Yoo**[1], **Sarah Sherman**[1], **Pinku Mukherjee**[2], **Alana Ross**[1], **Pamela Pantazopoulos**[1], **Victoria Petkova**[3], **Christian Farrar**[4], **Zdravka Medarova**[1], and **Anna Moore**[1]

[1]Molecular Imaging Laboratory, MGH/MIT/HMS Athinoula A. Martinos Center for Biomedical Imaging, Department of Radiology, Massachusetts General Hospital and Harvard Medical School, Charlestown, MA

[2]Department of Biological Sciences, University of North Carolina at Charlotte, Charlotte and School of Medicine, University of North Carolina at Chapel Hill, Chapel Hill, NC

[3]Molecular Medicine Core, Beth Israel Deaconess Medical Center, Harvard Medical School, Boston, MA

[4]MGH/MIT/HMS Athinoula A. Martinos Center for Biomedical Imaging, Department of Radiology, Massachusetts General Hospital and Harvard Medical School, Charlestown, MA

Abstract

The underglycosylated mucin 1 tumor antigen (uMUC1) is a biomarker that forecasts the progression of adenocarcinomas. In this study, we evaluated the utility of a dual-modality molecular imaging approach based on targeting uMUC1 for monitoring chemotherapeutic response in a transgenic murine model of pancreatic cancer (KCM triple transgenic mice). An uMUC1-specific contrast agent (MN-EPPT) was synthesized for use with magnetic resonance imaging (MRI) and fluorescence optical imaging. It consisted of dextran-coated iron oxide nanoparticles conjugated to the near infrared fluorescent dye Cy5.5 and to a uMUC1-specific peptide (EPPT). KCM triple transgenic mice were given gemcitabine as chemotherapy while control animals received saline injections following the same schedule. Changes in uMUC1 levels following chemotherapy were monitored using T2-weighted MRI and optical imaging before and 24 hr after injection of the MN-EPPT. uMUC1 expression in tumors from both groups was evaluated by histology and qRT-PCR. We observed that the average delta-T2 in the gemcitabine-treated group was significantly reduced compared to the control group indicating lower accumulation of MN-EPPT, and correspondingly, a lower level of uMUC1 expression. *In vivo* optical imaging confirmed the MRI findings. Fluorescence microscopy of pancreatic tumor sections showed a lower level of uMUC1 expression in the gemcitabine-treated group compared to the control, which was confirmed by qRT-PCR. Our data proved that changes in uMUC1

Correspondence to: Anna Moore, Ph.D., Professor of Radiology, Molecular Imaging Laboratory, MGH/MIT/HMS Athinoula A. Martinos Center for Biomedical Imaging, Department of Radiology, Massachusetts General Hospital and Harvard Medical School, 13th St., Boston, MA 02129, USA, Tel.: 1617-724-0540, Fax: 1617-643-4865, amoore@helix.mgh.harvard.edu or Zdravka Medarova, Ph.D., Assistant Professor of Radiology, Molecular Imaging Laboratory, MGH/MIT/HMS Athinoula A. Martinos Center for Biomedical Imaging, Department of Radiology, Massachusetts General Hospital and Harvard Medical School, 13th St., Boston, MA 02129, USA, Tel.: 1617-724-0540, Fax: 1617-643-4865, zmedarova@partners.org.
P.W. and B.Y. contributed equally to this work

Additional Supporting Information may be found in the online version of this article.

expression after gemcitabine chemotherapy could be evaluated using MN-EPPT-enhanced *in vivo* MR and optical imaging. These results suggest that the uMUC1-targeted imaging approach could provide a useful tool for the predictive assessment of therapeutic response.

Keywords

underglycosylated mucin 1 tumor antigen (uMUC1); pancreatic cancer; in vivo imaging; nanoparticles

---

It is becoming clear that, in the course of therapeutic intervention, cancer cells undergo specific molecular transformations long before there is a detectable change in tumor morphology or physiology. The ability to detect and analyze the response to therapy at these earliest stages of molecular dysregulation, before any overt physiologic symptoms have developed, would permit much more adequate therapeutic intervention and would represent an additional step in the direction of transforming cancer into a curable disease. The conception of molecularly targeted diagnostic approaches would be very valuable toward this goal because the ability to predict an individual patient's response to therapy would make therapeutic intervention much more effective and efficient. Such approaches would move us closer to the realization of precision medicine in its truest form.

Our search for biomarkers that forecast the progression of adenocarcinoma identified the underglycosylated mucin 1 tumor antigen (uMUC1) as a potential candidate. uMUC1 is overexpressed and underglycosylated on over 50% of human cancers. Its abundance appears to be tightly linked to tumor progression from premalignancy to advanced malignancy, as well as to tumor response to chemotherapy.[–]

The uMUC1 biomarker is highly clinically relevant. In our earlier studies, analysis of uMUC1 gene expression and protein abundance in human biopsy samples from breast cancer patients revealed a marked upregulation of the antigen in the adjacent normal tissues of all patients relative to tissues from women with no cancer history. This altered expression was accompanied by post-translational modifications characteristic of oncogenic transformation, *e.g.*, basolateral glandular distribution and cytosolic cellular localization. These molecular abnormalities in seemingly "normal" tissue, as defined by standard histopathology, indicate that uMUC1 is altered very early in the process of breast carcinogenesis and could serve as a predictive biomarker of cancer progression.

It is highly desirable to develop a noninvasive technique to image the changes of uMUC1 expression.[,] To probe for uMUC1 dysregulation using noninvasive imaging, we have previously designed and synthesized a contrast agent (MN-EPPT) that consists of iron oxide nanoparticles (MN, detectable by magnetic resonance imaging, MRI) conjugated to peptides (EPPT), specific for uMUC1. We have shown that MN-EPPT accumulation in tumors mirrors the abundance of uMUC1 and is suitable for the tracking of change in tumor size following chemotherapy in orthotopic murine models of pancreatic and breast cancer.[,]

More importantly, we have developed a method for the quantitative assessment of uMUC1 expression in breast tumors using noninvasive MRI. Specifically, we have shown that

treatment with doxorubicin in an orthotopic mouse model of breast cancer led to downregulation of the uMUC1 antigen in the tumors. Ultimately, we provided proof-of-principle that MN-EPPT-enhanced MRI and optical imaging could detect these changes in uMUC1 expression *in vivo*, establishing a molecular biomarker of chemotherapeutic response.

Our further investigation into uMUC1 biology using noninvasive MRI in a transgenic mouse model of breast cancer revealed that this antigen is already altered in the premalignant stage. This indicated that targeting uMUC1 with MN-EPPT could be used for monitoring premalignant transformation in the mammary fat pad. Our noninvasive approach was also valuable for detecting changes in uMUC1 expression during chemotherapy with doxorubicin in this transgenic model, which caused uMUC1 downregulation.

As uMUC1 expression has global relevance in adenocarcinomas including pancreatic cancer, this study focused on applying our imaging approach to pancreatic cancer, as it has the lowest survival rate among all common cancers. We utilized a genetically engineered mouse model that spontaneously induced human uMUC1-positive pancreatic cancer,[9] and evaluated changes in uMUC1 expression in response to gemcitabine chemotherapy using MN-EPPT-enhanced MRI and correlative optical imaging. Our results show that assessment of therapeutic response based on uMUC1 downregulation is not restricted to breast cancer,[9] but may be indicative of a global early response of adenocarcinoma cells to proapoptotic triggers. Finally, these new results suggest that the described imaging approach could provide a useful tool for the predictive assessment of therapeutic response.

Material and Methods

Animals and chemotherapy

All animal experiments were performed in compliance with institutional guidelines and approved by the Massachusetts General Hospital (MGH) and University of North Carolina Institutional Animal Care and Use Committees. To generate a human uMUC1-expressing mouse model of pancreatic cancer, first KC mice were generated on the C57BL/6 background by mating P48-Cre with LSL-KRASG12D mice. They were further mated to MUC1.Tg mice to generate KCM mice. Studies were initiated when the animals had an average age of 24.5 weeks (treated experimental, $n = 4$) and 23 weeks (nontreated controls, $n = 4$). The experimental mice were given treatment (gemcitabine, 20 mg/kg. i.p.) twice weekly for 10 weeks. The control mice received saline IP injections of the same amount at the same time (Table 1).

MN-EPPT synthesis

Nine grams of Dextan-T10 (Pharmacosmos, Holbaek, Denmark) was dissolved in 30 ml of double-distilled water and stirred in a round bottom flask on ice. $FeCl_3$ $6H_2O$ (0.65 g, Sigma-Aldrich, St. Louis, MO) was added while flushing Ar gas into the reaction mixture for an hour. $FeCl_2 \cdot 4H_2O$ (0.4 g, Sigma-Aldrich, St. Louis, MO) was added into the mixture and then 15 ml of concentrated cold NH_4OH (~28%, Sigma-Aldrich, St. Louis, MO) was added dropwise to the stirring mixture. The temperature was increased to 85°C for an hour

to induce the formation of a nanoparticulate colloidal mixture, cooled to room temperature and concentrated to 20 ml using Amicon Ultra centrifugal units (MWCO 30 kDa; Millipore, Billerica, MA). The resulting 20 ml dextran-coated magnetic nanoparticles (MN) were crosslinked and aminated with the subsequent addition of 35 ml of 5 M NaOH, 14 ml of concentrated epichlorohydrin (8 h, Sigma-Aldrich, St. Louis, MO) and 60 ml of concentrated NH_4OH. The nanoparticle solution was purified using a dialysis bag (MWCO 14 kDa) against water and 20 mM citrate buffer (pH 8.0) and then concentrated to 20 ml by Amicon Ultra centrifugal unit (EMD Millipore, Billerica, MA). The nanoparticle concentration was determined by iron assay, and the size of the nanoparticles was determined by dynamic light scattering (Zetasizer Nano ZS, Malvern Instruments, Malvern, UK).

Cy5.5 monoreactive NHS ester (1 mg, GE Healthcare, Piscataway, NJ) was dissolved in 100 μl of anhydrous DMSO and incubated with MN (10 mg Fe) in 20 mM citrate buffer (pH 8.0) overnight. The nanoparticles were purified using Sephadex PD-10 column (GE Healthcare, Piscataway, NJ) with PBS eluent. The number of Cy5.5 molecules per nanoparticle was determined to be four Cy5.5 molecules per MN by spectrophotometry. Cy5.5-labeled MN (MN-Cy5.5) were loaded with heterobifunctional crosslinkers, *N*-γ-maleimidobutyryl-oxysuccinimide ester (GMBS, Pierce Biotechnology, Rockford, IL) and conjugated with EPPT peptide. Briefly, 2.4 mg (20.7 nmol) of MN-Cy5.5 was reacted with 0.625 mg (100 equiv) of GMBS in PBS (pH 8.0) overnight at 4°C and subsequently purified on a PD-10 column. GMBS-MN-Cy5.5 was conjugated with EPPT peptide (96 nmol, 15 equiv), modified with a thiol group at its N-terminus (NH2-Cys-(PEG)-Tyr-Cys(acm)-Ala-Arg-Glu-Pro-Pro-Thr-Arg-Thr-Phe-Ala-Tyr-Trp-Gly-Lys-$CONH_2$) for the selective conjugation with maleimide on MN. The amount of EPPT peptide on MN was quantified by BCA protein assay (Pierce Biotechnology, Rockford, IL) and iron assay to confirm the loading ratio of EPPT peptide/MN/Cy5.5 (8.7/1/2.3).

Magnetic resonance imaging

In vivo MRI was performed using a 9.4T Bruker horizontal bore scanner equipped with a Rat Array MRI CryoProbes coil (Bruker, Billerica, MA). Multi-slice multi-echo T2-weighted maps of a mouse abdomen were obtained with the following parameters: TR = 2,000 msec/TE = 8, 16, 24, 32, 40, 48, 56, 64, 72, 80 msec; slice orientation: axial; number of averages (NA) = 2, rapid acquisition with relaxation enhancement factor = 8; FOV = 4.0 cm^2, matrix size 128, spatial resolution 312 mm^2, slice thickness = 0.5 mm, flip angle = 180°, resolution read = 0.025 cm/pixel and scan time = 8 min 32 sec. T2 maps were collected on weeks 3, 5, 7, 11, 12 and 13 after the beginning of chemotherapy (Fig. 1). Image analysis was performed by two independent investigators blinded to sample identity (sample size: treated experimental, $n = 4$ and nontreated controls, $n = 4$). T2 maps were analyzed voxel-by-voxel by fitting the T2 measurements to a standard exponential decay curve, defined by the following equation: $y = A \exp(-t/T2)$ using MATLAB software R2011b (The MathWorks, Inc., Natick, MA). Average T2 times in free-hand selected region of interests (ROIs) surrounding the targeted pancreatic sections were calculated using ImageJ software 1.50c (NIH, Bethesda, MD). MRI of experimental and control mice was performed before (precontrast) and 24 hr after (postcontrast) intravenous injection of the

MN-EPPT (15 mg Fe/kg of body weight). Delta-T2 values were calculated as T2 precontrast – T2 postcontrast and were used as an indicator of relative MN-EPPT accumulation.

Epifluorescence optical imaging

Epifluorescence optical imaging was performed on weeks 10, 11, 13 and 26 after the beginning of therapy with gemcitabine (Fig. 1). Images from the animals were obtained 24 hr after intravenous injection of the MN-EPPT probe using an IVIS Spectrum animal imaging system (PerkinElmer, Hopkinton, MA) with specific filters for the Cy5.5 dye on the MN-EPPT probe. Imaging was performed over the midsection of the body centered on the pancreas. Image analysis was conducted using LivingImage 4.2 software (PerkinElmer, Hopkinton, MA). To evaluate imaging results, an ROI was drawn around the selected tissue. Average fluorescence signal efficiency, which is defined as fluorescence emission normalized to the incident excitation intensity (radiance of the subject/illumination intensity), was used for quantification. Fluorescence efficiency was used as a measure of relative MN-EPPT accumulation.

qRT-PCR

Total RNA was extracted from frozen pancreatic tissue lysates using the Qiagen RNeasy Mini Kit (Qiagen, Valencia, CA). Taq-Man real-time PCR analysis was done using an ABI Prism 7700 sequence detection system (PE Applied Biosystems, Foster City, CA). The PCR primers and TaqMan probe specific for MUC1 mRNA were designed using Primer express software 1.5. Primer and probe sequences were as follows: forward primer, 5′-ACAGGTTCTGGTCATGCAAGC-3′; reverse primer, 5′-CTCACAGCATTCTTCTCAGTAGAGCT-3′; TaqMan probe, 5′-FAM-TGGAGAAAAGGAGACTTCGGCTACCCAGA-TAMRA-3′. Eukaryotic 18S rRNA TaqMan PDAR Endogenous Control reagent mixture (PE Applied Biosystems, Foster City, CA) was used to amplify 18S rRNA as a housekeeping control gene. At the RT step, incubation was done at 48°C for 30 min followed by 958C for 10 min for enzyme inactivation. The PCR amplification was run for 40 cycles at 95°C for 15 sec and at 60°C for 60 sec. Relative expression was calculated using the delta delta CT method. Two different pancreatic samples from each animal were analyzed in triplicate.

Histology

Immunohistochemistry staining was performed on mouse pancreatic frozen sections by staining for uMUC1 and co-localizing it with Cy5.5 signal derived from the MN-EPPT probe. Sections were stained with hamster monoclonal anti-mucin 1 antibody (MH1, 1:100 dilution; Pierce/Thermo Fisher, Carlsbad, CA), followed by incubation with corresponding FITC-labeled IgG secondary antibody (1:200 dilution; Abcam, Cambridge, MA) and counterstained with DAPI (Vectashield; Vector Laboratories, Inc., Burlingame, CA) for cell nucleus staining. The fluorescence images were examined using a Nikon Eclipse 50i fluorescence microscope (Nikon, Melville, NY), equipped with the necessary filter sets (Chroma Technology Corporation, Bellows Falls, VT). Images were acquired using a charge-coupled device camera with near infrared sensitivity (SPOT 7.4 Slider RTKE; Diagnostic Instruments, Sterling Heights, MI). Investigators blinded to the animal treatments evaluated all tissue sections using SPOT 4.0 Advance version software (Diagnostic

Instruments, Sterling Heights, MI). For histology comparison, the consecutive tissue sections were stained with hematoxylin and eosin (H&E).

Statistical analysis

Data are expressed as mean ± SD or SEM, where indicated. Statistical comparisons were evaluated by repeated-measures ANOVA. A value of $p < 0.05$ was considered statistically significant.

Results

MN-EPPT-enhanced molecular MRI permits the monitoring of therapeutic response

We hypothesized that changes in uMUC1 expression in pancreatic lesions after treatment with gemcitabine could be detected using MN-EPPT-enhanced *in vivo* imaging. This capability would provide a prognostic biomarker of therapeutic response. As seen in Figure 1, MRI permitted the stratification of animals based on treatment with gemcitabine. In gemcitabine-treated animals, there was a smaller change in T2 (delta-T2) than in nontreated animals ($p = 0.0008$). This indicated lower accumulation of MN-EPPT and, accordingly, lower levels of uMUC1 expression in gemcitabine-treated animals, consistent with our hypothesis. Importantly, this difference was seen as early as 7 weeks after the beginning of therapy at which point the mice were 30 weeks old—an age associated with early/moderate disease (pancreatic intraepithelial, PanIN lesions and carcinoma *in situ*, CIS).[9] The difference persisted after the discontinuation of treatment after week 10. Of note, one of the treated mice was classified as a nonresponder because the delta-T2 of its pancreas was consistently larger than that in the remaining treated animals starting at week 7 of treatment (Fig. 1). This indicated that gemcitabine had no effect on downregulation of uMUC1 in that animal. While this animal was clearly an outlier in this study, we chose to present these results as they might reflect a clinical situation when a patient does not respond to treatment. This may be the result of a more aggressive cell phenotype selected as a result of treatment with cytotoxic therapies, causing a higher level of uMUC1. Indeed, tumor aggressiveness and proliferation have long been associated with uMUC1 overexpression in cancer cells,[9] which could explain the higher delta-T2 in the case of the nonresponder animal.

MN-EPPT-enhanced molecular optical imaging permits the monitoring of therapeutic response

The findings from MRI were confirmed by *in vivo* epifluorescence optical imaging. This independent imaging modality was made possible by the presence of the Cy5.5 dye on the MN-EPPT probe. Figure 2 presents images collected at the end of treatment with gemcitabine (week 10) and for 2 weeks after the end of treatment. Fluorescence intensity associated with the pancreas of the nontreated animals remained visibly higher than in the gemcitabine-treated animals. This indicated persistently higher accumulation of MN-EPPT and, correspondingly, higher expression levels of uMUC1. Importantly, this difference was retained as late as week 26 after the beginning of treatment (Fig. 3). At that point, the animals had not been treated with chemotherapy for 13 weeks and were 49 weeks old, an age associated with high-grade disease. This observation suggested that the described

imaging method could be useful for the long-term monitoring of disease progression, possibly providing an avenue for the early detection of recurrence or tumor growth arrest.

In addition, the observed lack of response in one of the treated animals, as demonstrated by MRI, was paralleled by fluorescence optical imaging. As shown in Figure 4, the same mouse that presented with abnormally large delta-T2 values on MRI (Fig. 1) had high levels of fluorescence associated with the pancreas on optical imaging. This manifestation was similar to the nontreated controls and visibly different from the treated animals that responded to treatment, in which fluorescence intensity was lower (Fig. 4). The agreement between MRI and optical imaging indicates that the observed results indeed reflected differences in the accumulation of the MN-EPPT probe and that these differences could be considered as a surrogate for therapeutic outcome.

Ex vivo analysis validates the capacity of the MN-EPPT probe to detect changes in uMUC1 expression after treatment with gemcitabine

To corroborate the differences in tissue transformation between animals treated with gemcitabine and nontreated controls, we performed histopathological analysis of pancreatic sections derived from the study animals 26 weeks after the beginning of treatment. The prevalent glandular structure in gemcitabine-treated animals was normal (Supporting Information Fig. 1). In control, nontreated animals, there was clear evidence of high-grade PanIN lesions and CIS, associated with disorganized glandular epithelium. The histopathological appearance of the nontreated animals was indistinguishable from that of the nonresponder identified through imaging (Supporting Information Fig. 1).

To confirm the specificity of the MN-EPPT probe for uMUC1, we performed *ex vivo* histological immunostaining analysis of pancreatic sections from experimental and control animals. *Ex vivo* histology of pancreata derived from non-treated control animals revealed high expression of uMUC1 (as indicated by anti-uMUC1 staining) distributed throughout the disorganized glandular epithelium of PanIN lesions. The accumulation of MN-EPPT, indicated by the Cy5.5 signal from the probes, mirrored the distribution of uMUC1. By contrast, uMUC1 expression in the pancreatic lesions from the experimental group was lower and restricted to the apical membrane of the glandular epithelium. In addition, Cy5.5 signal from the MN-EPPT probe was low and limited to the apical glandular surface in the pancreatic tissues of experimental mice (Fig. 5 and Supporting Information Fig. 2). We also performed histological analysis of pancreatic sections from the nonresponder mouse identified by MRI and optical imaging. As expected (Fig. 5), immunostaining revealed a high expression of uMUC1 in the disorganized glandular epithelium and correspondingly high accumulation of MN-EPPT (Fig. 5 and Supporting Information Fig. 2). Finally, the differential expression of uMUC1 between non-treated and treated animals was confirmed by qRT-PCR (Supporting Information Fig. 3), lending further credence to the hypothesis that the accumulation of the MN-EPPT probe in these animals reflects uMUC1 expression.

Discussion

The ability to monitor cancer progression on a molecular level not defined by the presence of a palpable tumor mass and before any overt physiologic symptoms have developed would

permit early and more adequate therapeutic intervention. This article addresses this need by examining the possibility of predictive diagnostics for therapeutic response in a genetically engineered mouse model of pancreatic cancer. Specifically, we illustrate the monitoring of therapeutic response by detecting the changes in the expression profile of the molecular biomarker uMUC1 with a noninvasive imaging approach. By focusing on early disease, i.e., the PanIN lesion, we explore a scenario in which these molecular changes precede changes in other anatomical and physiologic signs of therapeutic progress.

This study extends our prior work in breast cancer, which demonstrated that treatment with doxorubicin resulted in downregulation of the uMUC1 antigen, and that MN-EPPT-enhanced MRI and optical imaging could detect changes in uMUC1 expression *in vivo*. By broadening the application of this methodology to pancreatic cancer, we move closer to establishing the value of uMUC1 as a wide-ranging predictive cancer biomarker. Based on our results from our previous and current studies we believe that uMUC1 downregulation is not caused by the specific action of doxorubicin or gemcitabine, but manifests itself as a generalized response of the tumor cell to a proapoptotic/cytostatic trigger provided by a chemotherapeutic drug. Determination of the precise molecular mechanism behind this observation, however, is outside the scope of this investigation and will be reported on separately.

Progress has already been made in the direction of predictive cancer diagnostics. An example includes screening for the BRCA mutation for the assessment of breast cancer risk. In most cases, however, cancer diagnostics is still focused on early rather than predictive detection. With specific regard to noninvasive imaging, a glimpse into the potential of this technology can be derived from the development of dynamic MRI techniques, magnetic resonance spectroscopy and positron emission tomography. Still, none of these technologies probe for specific molecular biomarkers expressed by cells in proportion to their potential for malignancy. Consequently, it is this highly specific molecular imaging approach that has the potential for capturing the earliest signs of therapeutic response and permitting predictive rather than curative therapeutic intervention.

Supplementary Material

Refer to Web version on PubMed Central for supplementary material.

Acknowledgments

National Institute of Health; Grant numbers: R01CA135650, R01CA163461

References

1. Strous GJ, Dekker J. Mucin-type glycoproteins. Crit Rev Biochem Mol Biol. 1992; 27:57–92. [PubMed: 1727693]
2. Ren J, Agata N, Chen D, et al. Human MUC1 carcinoma-associated protein confers resistance to genotoxic anticancer agents. Cancer Cell. 2004; 5:163–75. [PubMed: 14998492]
3. Siragusa M, Zerilli M, Iovino F, et al. MUC1 oncoprotein promotes refractoriness to chemotherapy in thyroid cancer cells. Cancer Res. 2007; 67:5522–30. [PubMed: 17545635]

4. Ghosh SK, Pantazopoulos P, Medarova Z, et al. Expression of underglycosylated MUC1 antigen in cancerous and adjacent normal breast tissues. Clin Breast Cancer. 2013; 13:109–18. [PubMed: 23122537]
5. Pietersz GA, Wenjun L, Krauer K, et al. Comparison of the biological properties of two anti-mucin-1 antibodies prepared for imaging and therapy. Cancer Immunol Immunother. 1997; 44:323–8. [PubMed: 9298934]
6. Song X, Airan RD, Arifin DR, et al. Label-free in vivo molecular imaging of underglycosylated mucin-1 expression in tumour cells. Nat Commun. 2015; 6:6719. [PubMed: 25813863]
7. Moore A, Medarova Z, Potthast A, et al. In vivo targeting of underglycosylated MUC-1 tumor antigen using a multimodal imaging probe. Cancer Res. 2004; 64:1821–7. [PubMed: 14996745]
8. Medarova Z, Pham W, Kim Y, et al. In vivo imaging of tumor response to therapy using a dual-modality imaging strategy. Int J Cancer. 2006; 118:2796–802. [PubMed: 16385568]
9. Medarova Z, Rashkovetsky L, Pantazopoulos P, et al. Multiparametric monitoring of tumor response to chemotherapy by noninvasive imaging. Cancer Res. 2009; 69:1182–9. [PubMed: 19141648]
10. Ghosh SK, Uchida M, Yoo B, et al. Targeted imaging of breast tumor progression and therapeutic response in a human uMUC-1 expressing transgenic mouse model. Int J Cancer. 2013; 132:1860–7. [PubMed: 23015160]
11. Remmers N, Anderson JM, Linde EM, et al. Aberrant expression of mucin core proteins and o-linked glycans associated with progression of pancreatic cancer. Clin Cancer Res. 2013; 19:1981–93. [PubMed: 23446997]
12. Besmer DM, Curry JM, Roy LD, et al. Pancreatic ductal adenocarcinoma mice lacking mucin 1 have a profound defect in tumor growth and metastasis. Cancer Res. 2011; 71:4432–42. [PubMed: 21558393]
13. Tinder T, Subramani D, Basu G, et al. MUC1 enhances tumor progression and contributes toward immunosuppression in a mouse model of spontaneous pancreatic adenocarcinoma. J Immunol. 2008; 181:3116–25. [PubMed: 18713982]
14. Hakomori S. Glycosylation defining cancer malignancy: new wine in an old bottle. Proc Nat Acad Sci USA. 2002; 99:10231–3. [PubMed: 12149519]
15. Hollingsworth M, Swanson B. Mucins in cancer: protection and control of the cell surface. Nat Rev Cancer. 2004; 4:45–60. [PubMed: 14681689]
16. Bayraktar S, Gluck S. Systemic therapy options in BRCA mutation-associated breast cancer. Breast Cancer Res Treat. 2012; 135:355–66. [PubMed: 22791366]
17. Chang YC, Yu CJ, Chen CM, et al. Dynamic contrast-enhanced MRI in advanced nonsmall-cell lung cancer patients treated with first-line bevacizumab, gemcitabine, and cisplatin. J Magn Reson Imaging. 2012; 36:387–96. [PubMed: 22517425]
18. Kim MJ, Lee SJ, Lee JH, et al. Detection of rectal cancer and response to concurrent chemoradiotherapy by proton magnetic resonance spectroscopy. Magn Reson Imaging. 2012; 30:848–53. [PubMed: 22503087]
19. Strigari L, Attili A, Duggento A, et al. Quantitative analysis of basal and interim PET/CT images for predicting tumor recurrence in patients with Hodgkin's lymphoma. Nucl Med Commun. 2016; 37:16–22. [PubMed: 26440569]

What's new?

During treatment, cancer cells often undergo molecular changes long before tumor morphology changes. Biomarkers to detect these changes could enhance therapy by allowing earlier analysis. In this study in mice, the authors developed a non-invasive technique for imaging cellular levels of the tumor antigen uMUC1, which is overexpressed in more than 50% of all cancers. They found that uMUC1 expression drops when pancreatic cancer begins to respond to therapy. This imaging technique may allow the early assessment of tumor response and prognosis.

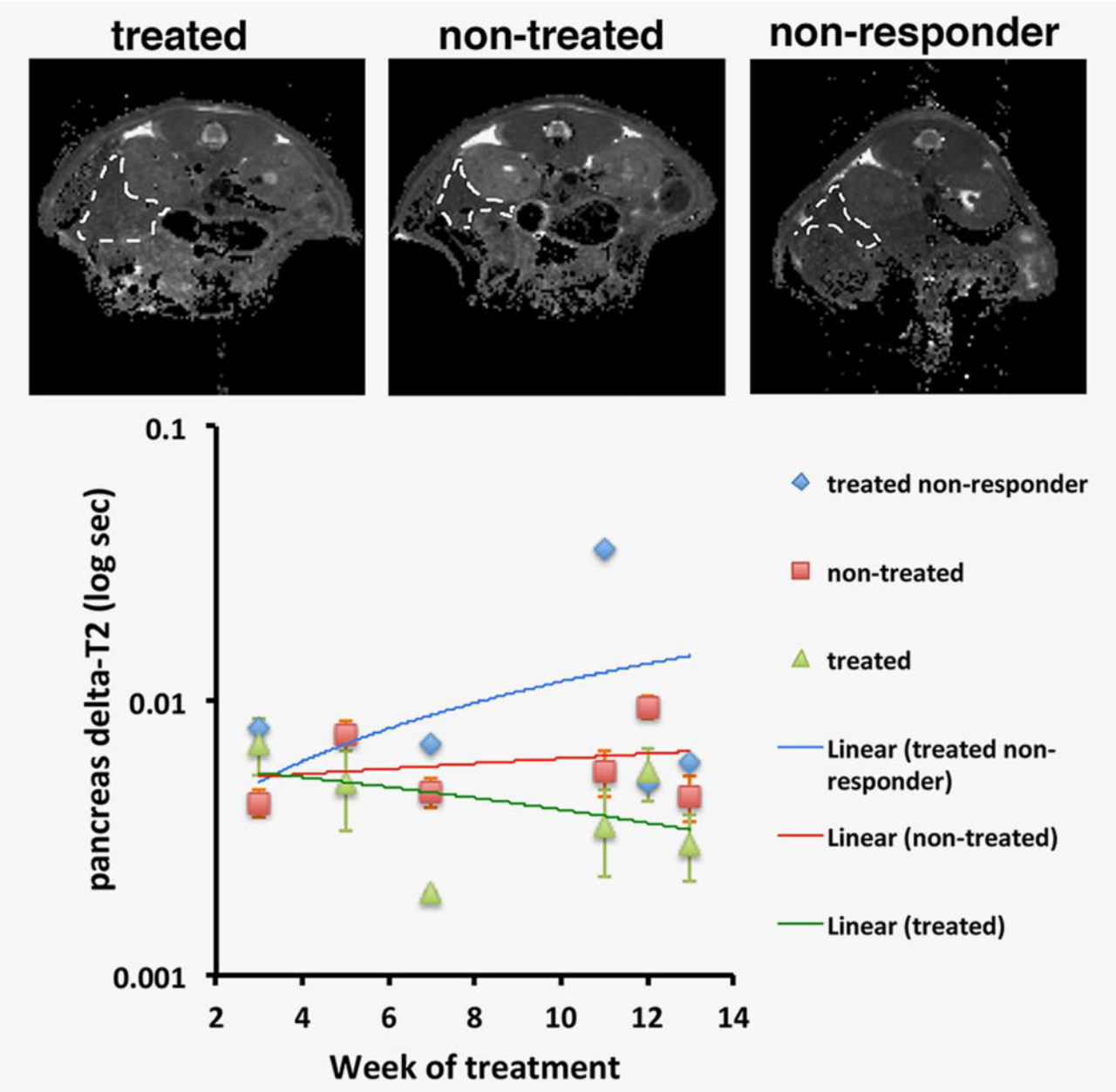

Figure 1.

MRI of therapeutic response. The animals were imaged by T2-weighted MRI from 3 to 13 weeks after the beginning of therapy with gemcitabine. Top—representative T2-weighted images (images were obtained on week 11 after the beginning of chemotherapy); bottom—quantitation of pancreas delta-T2 over time. Visible differences in contrast (top) and significant differences in delta-T2 (bottom) were apparent as early as 7 weeks after the beginning of therapy, except in one treated animal that presented with a high delta-T2 and was identified as a nonresponder ($p = 0.0008$; nontreated $n = 4$, treated $n = 3$; one-way repeated-measures ANOVA).

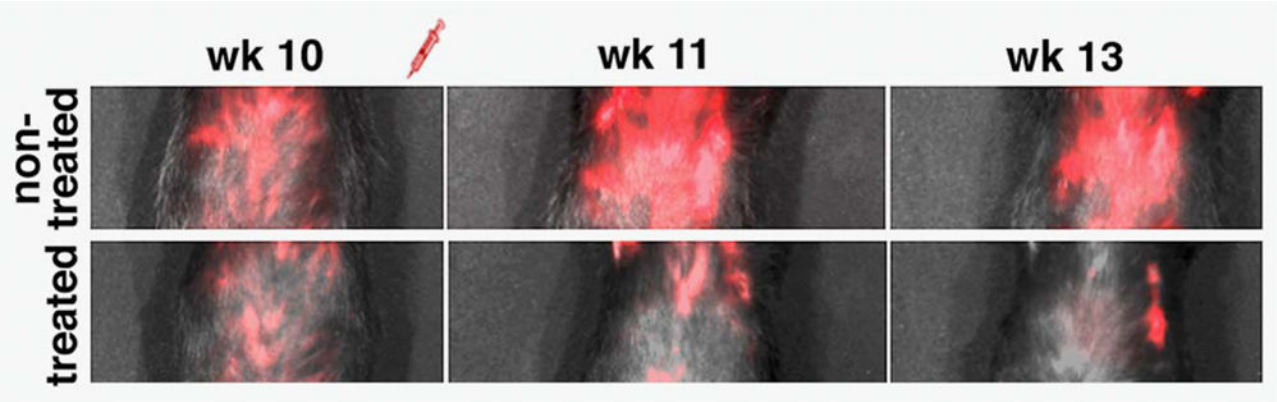

Figure 2.

Fluorescence optical imaging of therapeutic progress. The animals were imaged by epifluorescence optical imaging 10, 11 and 13 weeks after the beginning of therapy with gemcitabine. Visible differences in fluorescence intensity were apparent during the course of imaging.

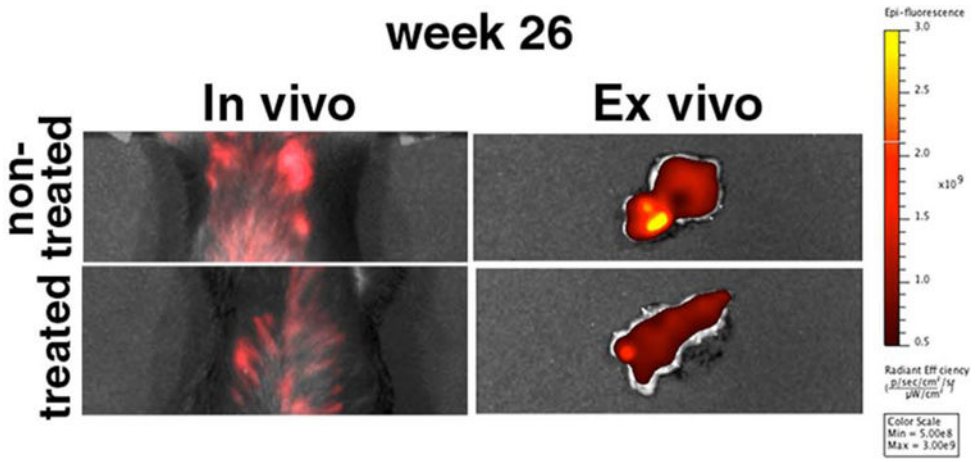

Figure 3.

In vivo and *ex vivo* optical imaging at the end of the study (week 26 after the beginning of therapy with gemcitabine). The visible differences in fluorescence intensity between treated and nontreated animals persisted even at that time point, 15 weeks after the end of chemotherapy.

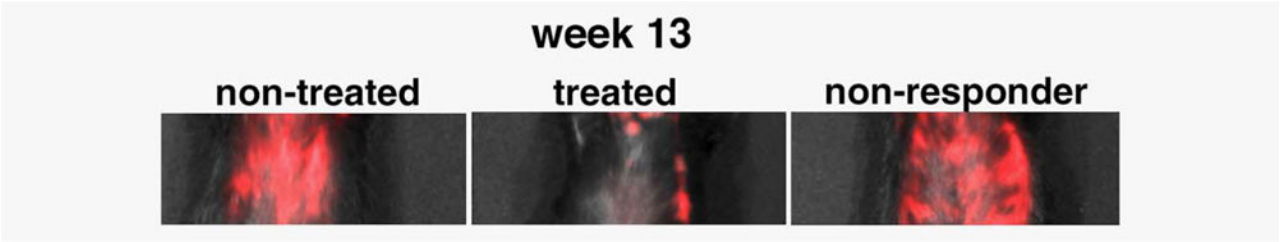

Figure 4.

In vivo optical imaging at the end point of therapy with gemcitabine. There were visible differences in fluorescence intensity between treated and nontreated animals, with the exception of one treated animal, which was classified as a nonresponder.

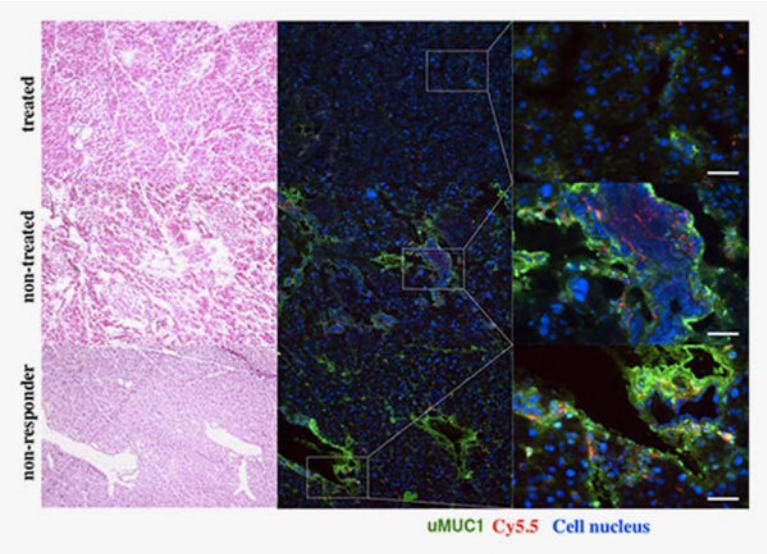

Figure 5.

Levels of uMUC1 in pancreatic sections of treated or non-treated animals. There was lower staining for uMUC1 in the pancreatic tissues of mice treated with gemcitabine relative to the control group. Accordingly, the accumulation of MN-EPPT reflected by the Cy 5.5 signal was notably decreased compared with the nontreated group. Immunostaining also identified the nonresponder, which had a high expression of uMUC1. uMUC1, green; Cy5.5, red; DAPI, blue; magnification bar = 30 μm. Consecutive sections were stained with H&E for histology correlation.

Table 1

Timeline for chemotherapy and imaging experiments

Week	1	2	3	4	5	6	7	8	9	10	11	12	13	26
Procedure														
Chemotherapy gemcitabine 20mg/kg i.p twice/week	◆	◆	◆	◆	◆	◆	◆	◆	◆	◆				
MR imaging pre and post contrast MN-EPPT 15mg/kg Fc i.v.			▲		▲		▲				▲	▲	▲	
Epifluorescencc optical imaging post contrast MN-EPPT 15mg/kg Fc: i v.										✸	✸		✸	✸
Sacrifice and histology														●

Int J Cancer. Author manuscript; available in PMC 2016 August 01.